Journal of Colloid and Interface Science 490 (2017) 174–180

Contents lists available at ScienceDirect

Journal of Colloid and Interface Science

journal homepage: www.elsevier.com/locate/jcis

Regular Article

Self-assembled hemispherical nanowell arrays for superhydrophobic antireflection coatings

Cheng-Yen Lin [a], Kun-Yi Andrew Lin [b], Tung-Wei Yang [a], Ying-Chu Chen [a], Hongta Yang [a,*]

[a] Department of Chemical Engineering, National Chung Hsing University, 145 Xingda Road, Taichung City 40227, Taiwan
[b] Department of Environmental Engineering, National Chung Hsing University, 145 Xingda Road, Taichung City 40227, Taiwan

GRAPHICAL ABSTRACT

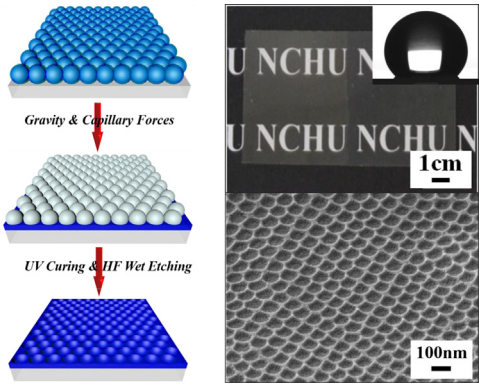

ARTICLE INFO

Article history:
Received 20 September 2016
Revised 14 November 2016
Accepted 19 November 2016
Available online 21 November 2016

Keywords:
Self-assembly
Colloidal crystals
Nanowell array
Antireflection
Self-cleaning

ABSTRACT

The present study reports an inexpensive and simple bottom-up technology for fabricating superhydrophobic antireflection coatings with highly ordered hemispherical nanowell structures, which are assembled by a scalable Langmuir-Blodgett technology. The subwavelength gratings lead to a gradual change in the effective refractive index, substantially suppressing specular reflection over the entire visible wavelength range. After surface modification with fluorinated silane, the resulting nanowell arrays exhibit superhydrophobic surface with high static water contact angle (154°) and low water contact angle hysteresis (7°). The experimental results on the wettability can be qualitatively interpreted by adopting the Cassie's dewetting model. Moreover, the effect of the nanowell shape on the antireflective and superhydrophobic properties has also been investigated in the study.

1. Introduction

In most optical applications, optical-grade polymers have replaced traditional optical glass owning to low cost of materials and high production volume with fast repeatability as well as high precision. The ever growing demand of polymer optics in areas as diverse as optical devices to consumer electronics has led to the search for ways to minimize the Fresnel's reflection at air/polymer interface, which could impair the legibility of displays and pose safety hazards [1–3]. To suppress the reflection, single quarter-wavelength antireflection coatings, multilayer antireflection coatings, and porous antireflection coatings are commonly applied to increase optical transmission [4–7]. However, the coating

* Corresponding author.
E-mail address: hyang@dragon.nchu.edu.tw (H. Yang).

http://dx.doi.org/10.1016/j.jcis.2016.11.064
0021-9797/

procedures usually require high cost and complex fabrication processes [8].

Periodic nanostructures in biological systems have inspired scientists to biomimic natural structures for practical applications [9,10]. A prominent case is the fabrication of subwavelength-structured moth-eye antireflection coatings, which consist of non-close-packed conical nipples [11]. The graded transition of effective refractive index between air and cornea leads to a superior broadband antireflection performance than single layer or multilayer coatings [12]. In addition, the gratings are more durable than multilayer antireflection coatings owning to no foreign material is involved. Moreover, inspired by the cicada wing, the resulting structures can be surface modified to achieve superhydrophobic property [13,14].

Currently, numerous top-down technologies, including photolithography, nanoimprint lithography, E-beam lithography, and interference lithography are applied to develop the subwavelength nipple arrays [15–18]. However, the technologies suffer from high cost of fabrication and low resolution of features. On the other hand, self-assembly of colloidal particles is a simple and inexpensive technology for creating highly ordered colloidal crystals, which can be used as templates to produce nipple arrays [19–21]. Nevertheless, the fabrication procedures involve either infiltration of matrix-forming materials or lithography-based technologies, which are still difficult to implement. Moreover, most of the bottom-up technologies involve multiple steps, and are favorable for low-volume laboratory-scale production only [22–24]. Recently, a one-pot evaporation-induced self-assembly of colloidal silica nanoparticles in the presence of monomer is applied to fabricate three-dimensional inverse opal structures [25]. Although three-dimensionally ordered porous structures can be attained using this method, the construction of large-area two-dimensional periodic structures has remained a substantial challenge.

Inspired by this methodology, we demonstrate scalable Langmuir Blodgett (LB) technology can be utilized for assembling monolayer silica colloidal crystals, partially embedded in polymer matrices, on polymer substrates directly in a signal step. The silica spheres can be removed to create periodic hemispherical nanowell arrays for antireflection coatings. The method is easily optimized for a large variety of substrates, including plastic plates, glass microslides, and silicon wafers [26]. Further advantage is that the resulting gratings exhibit superhydrophobic and self-cleaning through a surface modification procedure. This prevents scattering losses due to accumulation of water droplets.

2. Experimental section

2.1. Materials and substrates

The regents used for silica sphere synthesis, including tetraethyl orthosilicate (TEOS) (98%) and ammonium hydroxide (NH_4OH) (28%), are obtained from Sigma-Aldrich. Absolute ethanol (99.9%) is provided by Echo Chemicals. Deionized water (18.2 MΩ cm) is used directly from a Millipore A-10 water purification system. The UV-curable ethoxylated trimethylolpropane triacrylate monomer (ETPTA, SR 454) and photoinitiator, 2-hydroxy-2-methyl-1-phenyl-1-propanone (Darocur 1173), are purchased from Sartomer and BASF, respectively. (Tridecafluoro-1,1,2,2,-tetrahydrooctyl)-trichlorosilane (97%) used for surface modification is provided by Alfa Aesar. All chemicals and solvents are of reagent quality and are used without further purification except for TEOS, which is freshly distilled before use. Poly(ethylene terephthalate) (PET) films with thickness ranging from 0.09 to 0.11 mm (Wisegate Technology) are cleaned in deionized water, rinsed with absolute ethanol, and then dried in a steam of nitrogen.

2.2. Preparation of colloidal suspensions

Monodispersed silica spheres with 155 nm diameters are synthesized by the StÖber method [27]. In this study, distilled TEOS is rapidly added to a mixture of absolute ethanol, deionized water, and NH_4OH at ambient temperature for 12 h. The synthesized StÖber silica particles are purified in absolute ethanol by 5 centrifugation/redispersion cycles to completely remove impurities, such as unreacted TEOS, deionized water, and NH_4OH. The purified silica spheres are redispersed in non-volatile ETPTA monomers with 1 vol% Darocur 1173 as photoinitiator by using a Thermolyne vortex mixer. After filtration through a 5 μm syringe filter (Whatman) to remove any particle aggregates, the transparent silica colloidal suspensions are stored in an open vial in dark for one day to allow any residual ethanol to evaporate.

2.3. Fabrication of periodic nanowell arrays

Using a double-sided tape attached to a syringe pump, a cleaned PET film is immersed in a glass crystallizing dish containing deionized water. The as-prepared silica colloidal suspension is added dropwise to the deionized water surface. The ETPTA monomer-covered silica spheres spread rapidly to form a colloidal monolayer at the air/water interface. Due to high surface tension of water, the floating monomer-covered silica spheres can be self-assembled into two-dimensional close-packed colloidal crystals by the capillary interaction between neighboring silica spheres. By gently tapping the crystallizing dish to facilitate the merging of crystal domains, the crystalline quality of the colloid arrays can be improved. The PET film preimmersed in deionized water is then withdrawn vertically at a constant rate of ~5 cm/min using a syringe pump; meanwhile the floating colloidal crystals are transferred onto the PET substrate. The sample is transferred to a UV curing system and ETPTA monomer is photo-polymerized by exposure to UV radiation for 10 s using 20 W UV bench lamp (Blak-Ray® XX-20BLB) as a light source. In this work, the as-assembled colloidal crystals serve as templates to pattern arrays of nanowell structures directly on PET substrates. The templated silica spheres are finally removed by wet etching by a 2 vol% hydrofluoric acid aqueous solution, followed by washing in ethanol.

2.4. Surface modification of periodic nanowell arrays

The hydrophobicity of the nanowell array-coated PET film is further improved by surface modification using fluorinated silane with low surface energy through the well-establish silane coupling reaction [28]. The PET film is placed in a oven, on the bottom of which is dispensed an open vial within a small amount of (Trideca fluoro-1,1,2,2,-tetrahydrooctyl)-trichlorosilane. The oven is heated up to 120 °C to evaporate the fluorinated silane. The silane coupling agents can be hydrolyzed with moisture to form reactive silane groups and further condense with other fluorinated silanes on the surface of PET film [29].

2.5. Characterization

Scanning electron microscopy (SEM) is performed on a JEOL 6335F FEG-SEM. A thin layer of gold is sputtered onto the samples prior to imaging. A digital camera (Nikon Coolpix L810) is employed in recording images of the samples. Optical reflection and transmission spectra at normal incidence are achieved by an Ocean Optics HR4000 high-resolution fiber-optic UV–visible-near-IR spectrometer, and the cone angle of collection is less than 5°. The spectra were acquired by Ocean Optics Spectra Suite Spectroscopy Software over a wavelength range of 300–800 nm using Ocean Optics DT-MINI-2-B as a light source. The static water

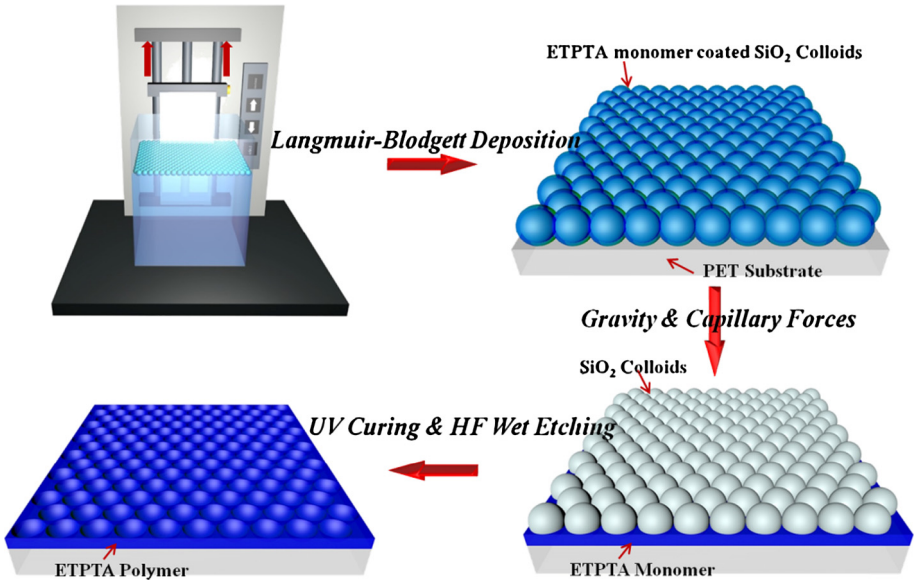

Fig. 1. Schematic illustration of the fabrication procedure for creating nanowell-structured antireflection coatings.

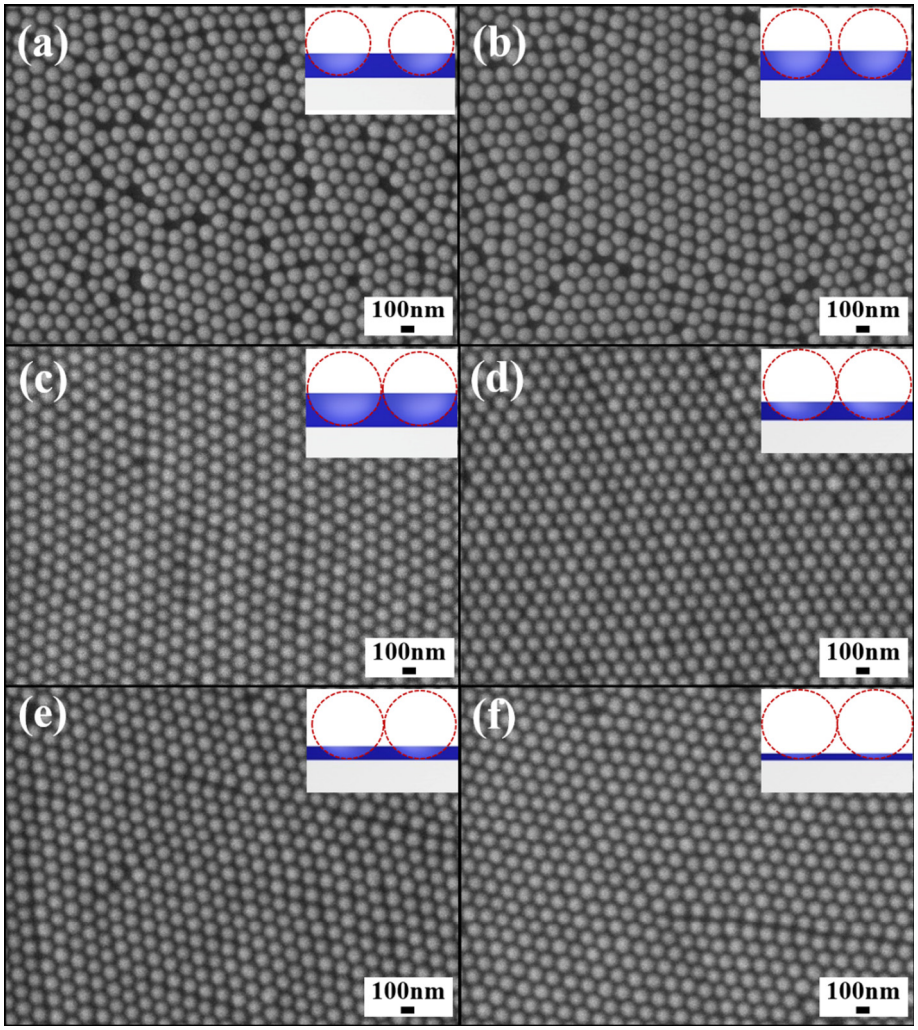

Fig. 2. Top-view SEM images of silica colloidal monolayers prepared using silica suspensions with different particle volume fractions. (a) 17.5 vol%. (b) 20.0 vol%. (c) 22.5 vol %. (d) 25.0 vol%. (e) 27.5 vol%. (f) 30.0 vol%.

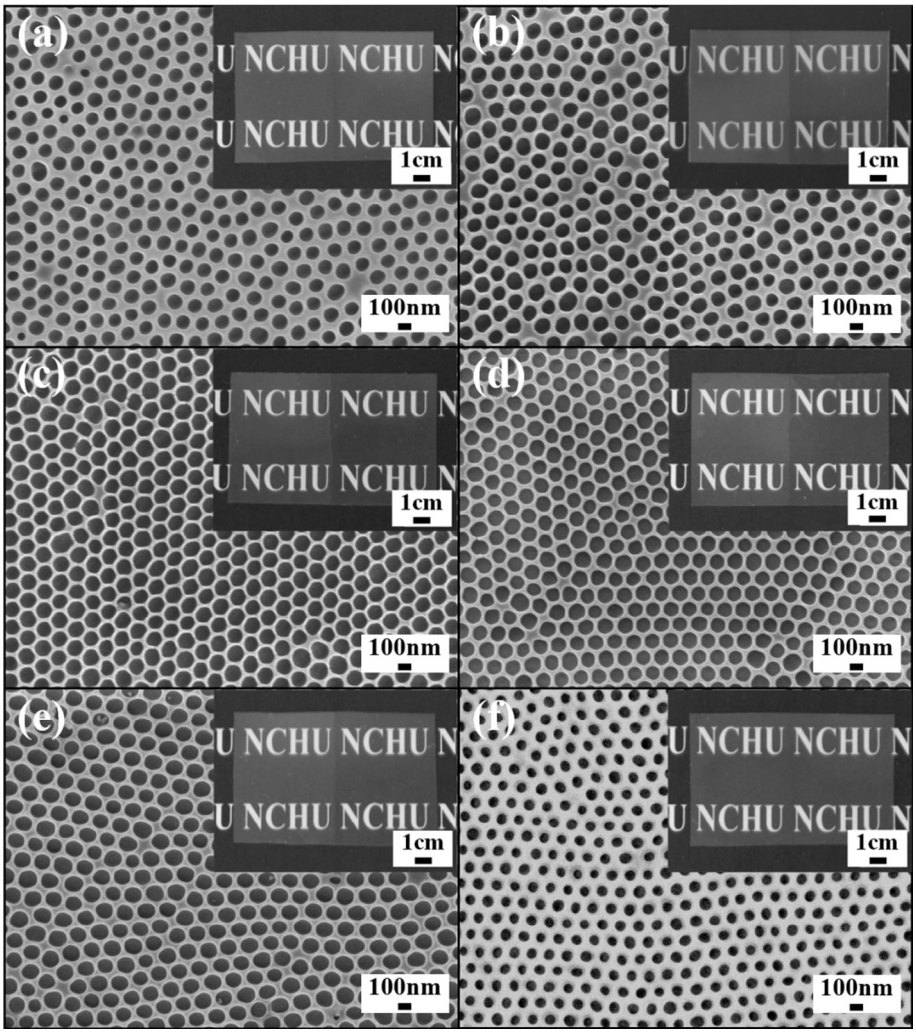

Fig. 3. Top-view SEM images of nanowell arrays prepared using silica suspensions with different particle volume fractions. (a) 17.5 vol%. (b) 20.0 vol%. (c) 22.5 vol%. (d) 25.0 vol%. (e) 27.5 vol%. (f) 30.0 vol%. Inserts showing photographic images of flat PET substrates (left) and PET substrates coated with the corresponding structures (right).

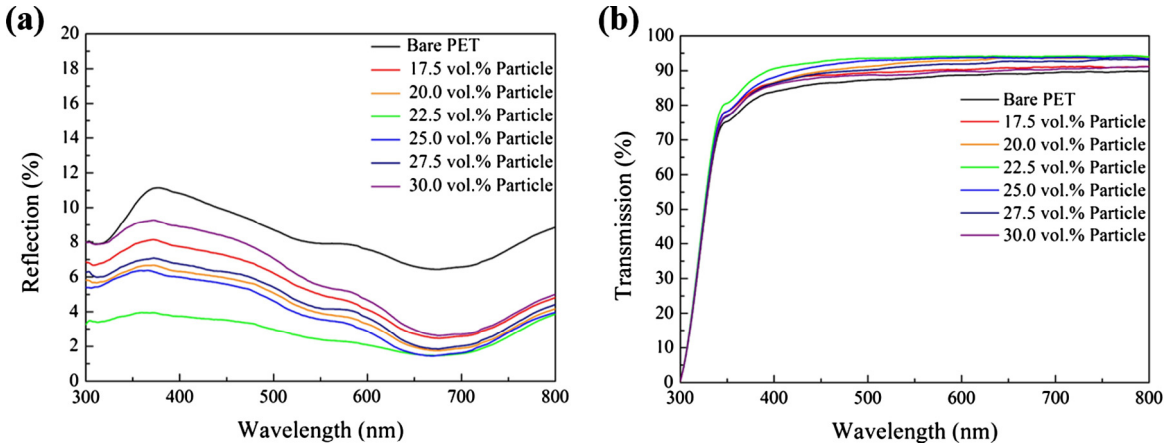

Fig. 4. (a) Normal incidence reflection spectra, and (b) normal incidence transmission spectra obtained from a flat PET substrate and PET substrates coated with nanowell arrays fabricated using silica suspensions with different particle volume fractions.

contact angles, advancing water contact angles, and receding water contact angles of the samples are measured using a sessile drop shape analysis system (KRÜSS G10) with auto-pipetting and imaging systems. A 10 μL deionized water drop is dispensed onto the sample surface using the auto-pipetting system, and an image of the drop is taken and then analyzed using DropSnake to collect a left and right contact angle. The DropSnake is an approach based on active contours to shape the water drop. This process is

repeated for 10 times on different regions for each sample, yielding 20 angle measurements per sample. The average of these measurements was reported as the water contact angle.

3. Results and discussion

Periodic polymer nanowell-structured antireflection coatings were created according to the self-assembly procedures presented in Fig. 1. In this LB deposition process, the ETPTA monomer-covered 155 nm silica spheres self-organized into close-packed ordering by tuning the surface tension of water with ETPTA monomer, instead of physical compression using mobile arms [27]. Monolayer of ETPTA monomer-covered silica colloidal crystals floating at the air/water interface were transferred onto the surface of PET substrate. During drying in air, the gravity and capillary action enabled the ETPTA monomers to flow and fill the empty space between the silica spheres and the PTE film. Importantly, no treatment, such as thermal annealing, was needed in this procedure. After completion of a photo-polymerization process, the embedded silica spheres were wet etched to fabricate periodic nanowell structures. The formation of UV-cured ETPTA polymer matrix results in the characteristic peaks assigned to acrylic C=C bonds of the ETPTA monomer disappear after the UV curing process (Fig. S1) [30].

Top-view SEM images of the LB assembled 155 nm silica colloidal crystals, partially embedded in ETPTA polymer matrices, using silica suspensions with different particle volume fractions (17.5, 20.0, 22.5, 25.0, 27.5, 30.0 vol%, respectively) are displayed in Fig. 2. The formation of a number of point vacancies, misaligned lines, and grain boundaries is apparent for the colloidal crystals prepared with a relatively low particle volume fraction suspension (Fig. 2(a)). The existence of defects decreases with increasing particle volume fraction of suspension (Fig. 2(b)). Moreover, as the particle volume fraction is above 22.5 vol%, long-range hexagonal ordering of close-packed silica colloidal crystals can be achieved (Fig. 2(c)–(f)). The packing of silica spheres sketches with various particle volume fractions are shown in the inserts of Fig. 2(a)–(f), respectively. Due to the refractive index matching between silica spheres and ETPTA monomer, the attractive van der Waals forces between assembled silica spheres are reduced as monomer fills the interspace [31,32]. Therefore, the usage of higher volume fraction monomer significantly disturbs the ordering of self-assembled silica spheres. In contrast to that, highly ordering close-packed silica sphere arrays are found as suspensions with higher particle volume fractions are introduced in the assembly process.

As shown in Fig. 3, nanowell structures are created after selective removal of the templating silica spheres. It is evident that the ordering of nanowell structure improves with the increasing of particle volume fraction (Fig. 3(a)–(c)). Comparing with that, the nanowell arrays are well preserved, and the void size decreases as the particle volume fraction increases from 22.5 vol% to 30.0 vol% (Fig. 3(c)–(f)). When the particles volume fraction reaches 22.5 vol%, the top hemispheres of silica spheres are exposed (Fig. 2(c)), leading to a maximum void size (150 ± 2 nm), which is close to the diameter of templating silica spheres. This further confirms the proposed mechanism we provide. The inserts of Fig. 3 display photographs of flat PET substrates (left) and nanowell-coated PET substrates (right) illuminated with white light. Comparing with bare PET substrate is translucent caused by Fresnel's reflection, the nanowell-coated PET substrates exhibit less milky color, where the "NCHU" underneath the coated substrates can be distinctly read. The transparent specimens demonstrate that less incident visible light is reflected from the nanowell-coated substrates, indicating that broadband antireflection coatings can be successfully prepared using the scalable LB assembly technology. Importantly, it is observed the nanowell array-coated PET substrate in Fig. 3(c) displays highest transparency.

To further comprehend the adjustable antireflection properties, an UV–visible-near-IR spectrometer is introduced to evaluate the optical properties at normal incidence. Fig. 4(a) discloses that the normal incidence reflection spectra obtained from a flat PET substrate and PET substrates coated with nanowell arrays as displayed in Fig. 3. Due to the discontinuity of the refractive index between air and PET substrates, the Fresnel reflection occurs at the air/PET interface, leading to a reflectivity of ca. 8%. Although the reflection of nanowell-coating substrate increases with particle volume fraction, the resulting coatings show lower reflection than that of a PET substrate. Moreover, it is validated that a less than 4% reflection can be achieved as the particle volume fraction reaches 22.5 vol%. On the other hand, the transmission of PET substrate increases from ca. 89% to 94% as coated with nanowell arrays fabricating using silica suspension with 22.5 vol% particle (Fig. 4(b)). It is worth mentioning that the reductions of the reflectivity in the wavelength range between 600 nm and 800 nm results from the tungsten halogen lamp exhibits lower luminous intensity over the range of wavelength (Fig. S2).

Since the size of nanowell structure is less than the incident visible light wavelength, the propagation of incident light is governed by the change of effective refractive index from air to the surface of nanowell structures. In the measurement, the nanowell densities are counted from Fig. 3, while the void sizes are measured by averaging 100 voids. Theoretically, the void size can be used to calculate the height of nanowell structure. The broadband antireflection properties of the templated gratings can then be explained by mapping the calculated effective refractive index across the height of hemispherical nanowell (77.5 nm). Fig. 5 reveals the effective refractive index of hemispherical nanowell arrays fabricated using a 22.5 vol% silica suspension increases gradually from 1.0 to ~1.47 and then to 1.58. Compare with other dotted lines, this refractive index gradient results in a low reflection over visible light wavelength range. To investigate the impact of nanowell size on antireflection performance, nanowell coatings are prepared using a 22.5 vol% 70 nm silica suspensions. As shown in Fig. S3(a), even though some defects are presented, each nanowell with an average void size of around 70 nm surrounded by six others can be observed. Fig. S3(b) compares the normal incidence transmission spectra obtained from a flat PET substrate and PET substrates coated with hemispherical 155 nm and 70 nm nanowell arrays as

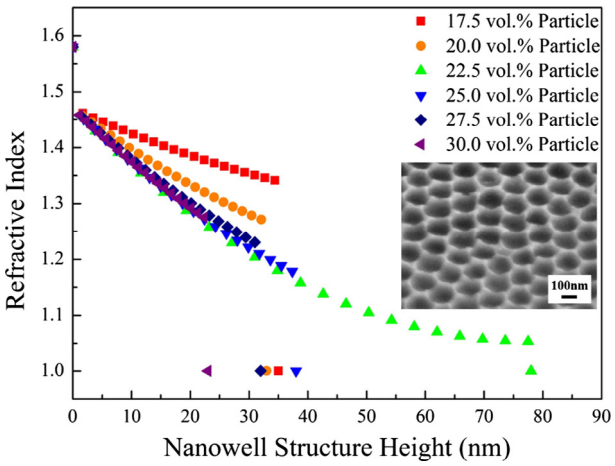

Fig. 5. Comparison of the change of calculated effective refractive index from PET substrate (height = 0) to the top of the templated nanowell structure. Insert showing a tilted-view SEM image of the nanowell arrays fabricated using a 22.5 vol % silica suspension.

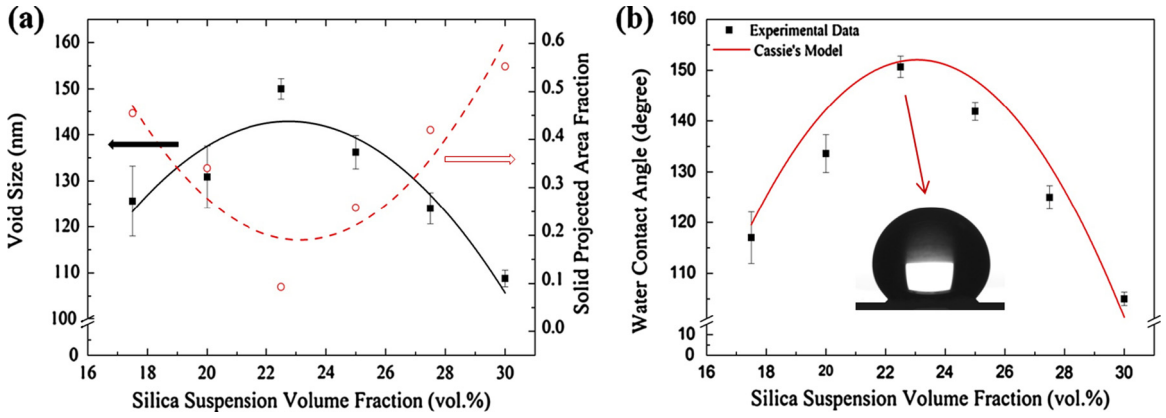

Fig. 6. (a) Dependence of the void size and the corresponding projected area fraction of surface modified nanowell arrays fabricated using silica suspensions with different particle volume fractions. (b) Experimental and calculated static water contact angles of the corresponding nanowell arrays.

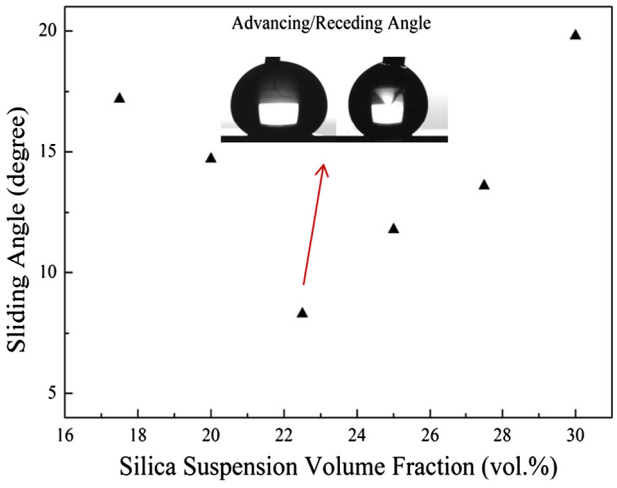

Fig. 7. Sliding angles for surface modified nanowell arrays fabricated using silica suspensions with different particle volume fractions.

displayed in Figs. 3(c) and S3(a). The 70 nm nanowell coating consistently presents higher transmittance (~95%) for the range of visible wavelengths than that of 155 nm nanowell coating (~94%), while the bare PET substrate displays lower transmittance (~90%) than those of nanowell coatings. Owing to larger structure size and inter-structure distance, part of the incident light rays are reflected at the 155 nm nanowell structure surface, and part of the rays are refracted and then lost by absorption within the structures or emerge after several internal reflections. Hence, the incident light in the form of propagating energy is scattered off. This indicates that smaller nanowell coating has slightly higher transmittance.

The as-assembled nanowell arrays can be directly used as superhydrophobic substrates after a surface functionalization with (Tridecafluoro-1,1,2,2,-tetrahydrooctyl)-trichlorosilane. The measured void sizes are summarized in Fig. 6(a). The results indicate that the void size increases with particle volume fraction in the beginning, and smaller void size is obtained as only bottom parts of the silica spheres are templated. By using the following calculation:

$$f = 1 - \left(\frac{\pi R_v^2}{2\sqrt{3}R_s^2}\right)$$

where R_v is the radius of voids and R_s is the radius of the templating 155 nm silica spheres. Since air can be trapped in the nanowells, the projected area fraction of the polymer in contact with a water droplet (f) can then be estimated as disclosed in Fig. 6(a). The theoretical static water contact angle on the surface modified coating can then be calculated by the Cassie's dewetting model:

$$\cos\theta' = f\cos\theta - (1 - f)$$

where θ' is the static water contact angle on a rough surface, θ is the intrinsic water contact angle on a flat surface. It is observed that the f value decreases with the increase of particle volume fraction, and reaches a minimum value as 22.5 vol% silica suspension is introduced. The calculated static water contact angles are compared with the experimental results in Fig. 6(b). It is clear that the experimental data follows similar tendency as the calculated results under different particle volume fractions, and the static water contact angle can reach a maximal contact angle of 152 ± 1° (inset of Fig. 6(b)). Furthermore, the sliding angle for the surface modified nanowell-coated PET substrate can achieve a minimum value of 7.7° (Fig. 7), indicating that superhydrophobic coatings with self-cleaning properties can be achieved.

4. Conclusions

In summary, we have developed a non-lithography-based approach that utilizes the self-organized and highly ordered silica spheres as templates to scalable fabricate periodic hemispherical nanowell structures in a single step. The resulting coatings exhibit broadband antireflection and superhydrophoic properties after a surface functionalization procedure, which are promising for creating self-cleaning antireflection coatings in a variety of important technological application in optical devices.

Acknowledgment

Acknowledgment is made to National Science Council – Taiwan (Grant No. MOST 104-2221-E-005-086) for support of this research.

Appendix A. Supplementary material

Supplementary data associated with this article can be found, in the online version, at http://dx.doi.org/10.1016/j.jcis.2016.11.064.

References

[1] M. Ibn-Elhaj, M. Schadt, Nature 410 (2001) 796.
[2] E. Hecht, Optics, third ed., Addison Wesley, 1998.
[3] H.A. Macleod, Thin-Film Optical Filters, second ed., McGraw-Hill, 1989.

[4] J. Hiller, H.D. Mendelsohn, M.F. Steiner, Nat. Mater. 1 (2002) 59.
[5] U. Schulz, Appl. Opt. 45 (2006) 1608.
[6] Y. Du, L.E. Luna, W.S. Tan, M.F. Rubner, R.E. Cohen, ACS Nano 4 (2010) 4308–4316.
[7] J.Y. Huang, X.D. Wang, Z.L. Wan, Nanotechnology 19 (2008) 025602.
[8] P.B. Clpham, M.C. Hutley, Nature 244 (1973) 281.
[9] M. Srinivasarao, Chem. Rev. 99 (1999) 1935.
[10] K.S. Liu, Y. Tian, L. Jiang, Prog. Mater. Sci. 58 (2013) 503.
[11] Y. Lai, F. Pan, C. Xu, H. Fuchs, L. Chi, Adv. Mater. 25 (2013) 1682.
[12] S. Chattopadhyay, L.C. Chen, K.H. Chen, Crit. Rev. Solid State Mater. Sci. 31 (2006) 15.
[13] J.W.M. Bush, D.L. Hu, Annu. Rev. Fluid Mech. 38 (2006) 339.
[14] Q.F. Xu, Y. Liu, F.J. Lin, B. Mondal, A.M. Lyons, ACS Appl. Mater. Interface 5 (2013) 8915.
[15] C. Heine, R.H. Morf, Appl. Opt. 34 (1995) 2476.
[16] Q. Chen, G. Hubbard, P.A. Shields, C. Liu, D.W.E. Allsopp, W.N. Wang, S. Abbott, Appl. Phys. Lett. 94 (2009) 26318.
[17] Y. Kanamori, M. Sasaki, K. Hane, Opt. Lett. 24 (1999) 1422.
[18] K.M. Baker, Appl. Opt. 38 (1999) 352.
[19] Y.-C. Chen, Z.-S. Huang, H. Yang, ACS Appl. Mater. Interfaces 7 (2015) 25495.
[20] M. Schmudde, C. Grunewald, C. Goroncy, C.N. Noufele, B. Stein, T. Risse, C. Graf, ACS Nano 10 (2016) 3525.
[21] W.-L. Min, B. Jiang, P. Jiang, Adv. Mater. 20 (2008) 3914.
[22] J. Zhu, Z.F. Yu, G.F. Burkhard, C.m. Hsu, S.T. Connor, Y.Q. Xu, Q. Wang, M. McGehee, S.H. Fan, Y. Cui, Nano Lett. 9 (2009) 279.
[23] B.P. Phillips, P. Jiang, B. Jiang, Appl. Phys. Lett. 99 (2011) 191103.
[24] J.-H. Kim, J.-H. Kim, K.-H. Choi, H.K. Yu, J.H. Kim, J.S. Lee, S.-Y. Lee, Nano Lett. 14 (2014) 4438.
[25] C. Warakulwit, S. Yadnum, C. Boonyuen, C. Wattanakit, A. Karajic, P. Garrigue, N. Mano, D. Bradshaw, J. Limtrakul, A. Kuhn, CrystEngComm 18 (2016) 5095.
[26] H. Yang, P. Jiang, J. Colloid Interface Sci. 405 (2013) 51.
[27] W. StÖber, A. Fink, J. Colloid Interface Sci. 26 (1968) 62.
[28] Y. Coffinier, S. Janel, A. Addad, R. Blossey, L. Gengembre, E. Payen, R. Boukherroub, Langmuir 23 (2007) 1686.
[29] E.P. Plueddemann, Silane Coupling Agents, second ed., Plenum Press, New York, 1991.
[30] K.H. Choi, S.J. Cho, S.H. Kim, Y.H. Kwon, J.Y. Kim, S.Y. Lee, Adv. Funct. Mater. 25 (2013) 1395.
[31] J.A. Lewis, J. Am. Ceram. Soc. 83 (2000) 2341.
[32] W.B. Russel, D.A. Saville, W.R. Schowalter, Colloidal Dispersions, Cambridge University Press, 1989.